Optimization and Engineering (2019) 20:151–177
https://doi.org/10.1007/s11081-018-9403-8

RESEARCH ARTICLE

Multi-objective optimization of the suspension system parameters of a full vehicle model

Giovani Gaiardo Fossati[1] · Letícia Fleck Fadel Miguel[1] · Walter Jesus Paucar Casas[1]

Received: 13 December 2017 / Revised: 13 June 2018 / Accepted: 10 September 2018 /
Published online: 28 September 2018

Abstract

The development of a methodology that enables the optimization of passive suspension system parameters, providing a group of optimal solutions, could be an excellent approach to obtain a fast improvement tool during the design of suspension systems. Thus, this paper proposes a methodology for the multi-objective optimization of the passive suspension system of a full-car model travelling in a random road profile. For this purpose, a numerical-computational routine is developed, which integrates the NSGA-II with the vertical dynamic analysis, in the time domain, of an eight degrees-of-freedom vehicle model with a seat. Three objective functions, which take into account passenger comfort and safety, are considered. The proposed methodology provides a Pareto-optimal front, which consists of a set of non-dominated solutions that minimize the three objective functions. Comparing the results of the dynamic analyses of the vehicle model with optimized and non-optimized suspension systems, it was verified that the optimization allowed a reduction of up to 21.14% of the weighted RMS value of the driver seat vertical acceleration, a parameter directly related to comfort, while maintaining or improving the trade-off with safety. The Pareto-optimal front has proven to be an excellent support tool to aid the designer in the determination of the parameters that best fit the suspension system to produce the desired dynamic behavior in vehicles. Thus, the proposed optimization methodology can be recommended as an effective tool for the optimal design of passive suspension system parameters. Finally, this work shows that the design of suspension parameters can be done taking into account passenger comfort and safety at same time.

Keywords Vehicle dynamics · Full-car model · Passive suspension system · NSGA-II · ISO 8608 · ISO 2631-1

✉ Letícia Fleck Fadel Miguel
letffm@ufrgs.br

Extended author information available on the last page of the article

1 Introduction

Increasingly, the automotive industry faces the challenge of combining maximum performance, safety and comfort with minimum cost, weight and production time. Thus, accurate numerical models of the vehicle, as well as a precise representation of the road network, have become imperative to reach the targeted quality standards for the manufacturing of vehicles and their components. Beyond the precision of numerical models, many situations still require the uncovering of the best possible parameters of the vehicle components to reach these quality standards, which can be obtained through an optimization algorithm. In addition, we may need to find the best option among conflicting characteristics, which requires a multi-objective optimization algorithm.

For instance, the optimization of a suspension system of a vehicle aiming to improve passenger comfort must not ignore parameters such as drivability, stability, safety and dimensional or other design requirements. It is not possible to improve all these simultaneously. Thus, the optimization in question is, by definition, a multi-objective problem, in which the improvement and deterioration of the vehicle features must be counterbalanced.

The development of a methodology that enables the optimization of passive suspension system parameters by providing to the designer a group of optimal solutions could be an excellent way to obtain a fast project improvement tool.

To carry out the proposed optimization, it is necessary to represent the road profile in the best possible way. A road surface representation using power spectral density (PSD) functions has been used by several authors, being that several modelling techniques were proposed previously or alternatively to the standardization of the method by the ISO 8608 (2016) standard. Authors such as Braun (1991) and Dodds and Robson (1973) proposed some of these modelling techniques, being a few methods and concepts used as theoretical background for the composition of such standard.

Shinozuka and Jan (1972) proposed a method for the digital simulation of random processes using PSD functions. This method proved to be an efficient tool for the generation of temporal signals, such as the vertical displacement of road surfaces, from the PSD functions, using equally spaced frequencies together with randomly generated phase angles that follow a uniform probability density distribution.

The ISO 2631-1 (1997) standard regulates whole-body-vibration evaluation methods, which give quantitative guidance on the effects of vibration associated with human health and comfort as well as on the perception and incidence of motion sickness.

Sekulic et al. (2013), adopting the ISO 2631-1 (1997) standard, studied the effects of vibrations on the comfort of intercity bus IK-301, in which the road profile PSD, representative of an asphalt-concrete road roughness, is generated as described by the Braun (1991) stochastic model. Gobbi (2013) and Gobbi et al. (2014), using genetic algorithms, carried out a multi-objective optimization of the suspension system of a quarter car vehicle model.

Deb et al. (2002) developed one of the most relevant variations of the genetic algorithm, called the non-dominated sorting genetic algorithm II (NSGA-II), which consists in a multi-objective meta-heuristic optimization algorithm that uses dominance and elitism concepts to obtain a non-dominated or Pareto-optimal front.

Gadhvi et al. (2016) performed a comparative study of the multi-objective optimization of the passive suspension of a half-car model using three of the most significant evolutionary algorithms: NSGA-II, the Strength Pareto Evolutionary Algorithm 2 (SPEA2) and the Pareto Envelope based Selection Algorithm II (PESA-II), showing that the three algorithms exhibit approximately the same performance. However, these authors observe better performance of NSGA-II in minimizing the objective vector, while SPEA2 and PESA-II tend to produce a more diversified Pareto-optimal front. NSGA-II is also the algorithm chosen by Nagarkar et al. (2016) and Shojaeefard et al. (2014) to obtain the Pareto-optimal front associated with the multi-objective optimization of the passive suspension system of a quarter-car model and a half-car model, respectively.

Numerous other approaches are able to solve the problem in question, and they generally diverge from the present work with respect to the algorithm and/or the vehicle model used and/or the simulation of the road profile. Some studies in the literature carry out a multi-objective optimization of a full-vehicle model travelling on a random road profile, but they do not provide a Pareto-optimal front as a set of optimal designs.

That being said, Drehmer et al. (2015) determined, through an analysis in the frequency domain, the aggregated suspension parameters that minimize a multi-objective function of a full-car model travelling on different road profiles. The authors used the human sensitivity curves proposed by the ISO 2631-1 (1997) standard to assess the vertical weighted RMS acceleration of the vehicle's driver seat. Additionally, authors such as Song et al. (2014), Meng et al. (2014), Xie et al. (2013) and Wang et al. (2010) solved the multi-objective optimization problem of the passive suspension system of a full-vehicle model with a seat through evolutionary algorithms based on competitive and cooperative game theory. The full-vehicle model used by these authors included the tire damping effect in the eight degrees-of-freedom (DOF) model proposed by Guclu (2005) in a study of the automotive vibration control using fuzzy logic.

Several authors have carried out multi-objective optimizations of vehicle models travelling on random road profiles, producing Pareto-optimal fronts, but they do not consider an 8-DOF full vehicle model in their analyses. Guo and Zhang (2017) consider a 7-DOF, a half-vehicle and a quarter-vehicle model in their study. Khalkhali et al. (2017), Shojaeefard et al. (2014) and Jamali et al. (2014) consider 5-DOF half-vehicle models. Nagarkar et al. (2016), Florea et al. (2016), Gobbi et al. (2006) and Gobbi and Mastinu (2001), in turn, use quarter-vehicle models.

Alternatively, Moradi et al. (2011) consider a full-vehicle model travelling on a random road profile, but carry out a single-objective optimization of the parameters. Finally, an extensive number of papers fulfill only one of the aspects of interest of the present study. Gadhvi et al. (2016) and Nariman-Zadeh et al. (2010) perform a multi-objective optimization and obtain the Pareto-optimal front of the passive suspension design of a 5-DOF half-vehicle model travelling on sinusoidal road

profiles. Abbas et al. (2013) transformed a multi-objective optimization into a single-objective problem by using weighting factors to obtain the optimal seat and suspension design of a half-car with driver, also subjected to a sinusoidal excitation.

Similarly, Shirahatt et al. (2008) optimized the aggregated parameters of the passive and active suspension systems of a full-car model with seat, which travels over a sinusoidal road profile, using two different metaheuristic algorithms. Shirahatt (2015) also compared the dynamic responses of a full-car model considering passive and active suspension systems when the vehicle model travels over random road profiles. Naudé and Snyman (2003a; b) used the LFOPC gradient-based algorithm to solve the single-objective optimization problem of a 6-DOF half-vehicle model travelling on a random road profile.

Thus, the main contribution of the present work is to propose a methodology for the multi-objective optimization, via NSGA-II, of the aggregated parameters of the passive suspension system of a full-vehicle model with a seat travelling on a random road profile, providing a Pareto-optimal front of the optimal designs as the output of the process. This front consists in the set of non-dominated solutions that minimize three objective functions: the weighted RMS value of the driver's seat vertical acceleration, the mean RMS value of the model wheels' dynamic amplification factor, and the maximum relative displacement between each wheel and the body of the vehicle model. The model represents a passenger car that travels at a constant speed on a random road profile provided by the ISO 8608 (2016) standard. Eight DOF adequately characterize the vertical dynamics of the full-vehicle model, which are determined in terms of vertical displacements, velocities and accelerations in a discrete time interval. All the routines are developed in Matlab.

2 Theoretical background

This section presents essential concepts and equations employed throughout the paper, which are fundamental elements of the methodology developed.

2.1 Multiple-track roughness simulation

The standardization of the road surface modelling methodology was accomplished by the ISO 8608 (2016) standard, which proposes a method of road profile representation through PSDs and provides general guidance for the use of statistical data, among further recommendations. According to ISO 8608 (2016), there is a logarithmic linear relation between the vertical displacement PSD and the spatial frequency of a given road profile, which can be defined as:

$$G_d(n) = G_d(n_0)\left(\frac{n}{n_0}\right)^{-w}, \tag{1}$$

in which $G_d(n)$ denotes the vertical displacement PSD in m^3, n is the spatial frequency in cycles/m, $G_d(n_0)$ is the reference vertical displacement PSD in m^3, n_0 is the reference spatial frequency in cycles/m and w is the wavelength distribution exponent. The spatial frequency ranges from 0.011 to 2.83 cycles/m, and the

reference spatial frequency, n_0, is defined by the standard as 0.1 cycle/m. The value for the wavelength distribution exponent, w, is usually defined as 2.

As stated by Sekulic et al. (2013), the vertical displacement PSDs in terms of spatial and temporal frequencies are related according to:

$$G_d(f) = \frac{G_d(n)}{v}, \tag{2}$$

in which $G_d(f)$ is the vertical displacement PSD in terms of temporal frequency in m^2 s, f is the temporal frequency in Hz and v is the vehicle speed in m/s. The spatial and temporal frequencies are associated according to:

$$f = n\,v. \tag{3}$$

In accordance with ISO 8608 (2016), the road's vertical velocity and acceleration PSDs can be obtained from the vertical displacement PSD through:

$$G_a(n) = G_v(n)\,(2\,\pi\,n)^2 = G_d(n)\,(2\,\pi\,n)^4, \tag{4}$$

in which $G_a(n)$ is the vertical acceleration PSD in m^{-1} and $G_v(n)$ is the vertical velocity PSD in m.

An expression that represents the road's vertical displacement PSD in terms of temporal frequency can be obtained by combining Eqs. (1)–(3):

$$G_d(f) = G_d(f_0)\left(\frac{f}{f_0}\right)^{-w}, \tag{5}$$

in which $G_d(f_0)$ is the reference vertical displacement PSD in m^2 s and f_0 is the reference temporal frequency in Hz.

Table 1, using information from ISO 8608 (2016), shows the geometric mean of the reference PSD for different classes of roads, which can provide an estimate of their roughness degree.

In multiple-track simulation, as in the case of a passenger car model which has four tires in contact with the ground, ISO 8608 (2016) highlights that it is convenient to consider that the road surface has the isotropy property. Thus, the vertical displacement PSDs of the road profiles in contact with the front left and front right tires of the vehicle model can be related through a coherence function:

Table 1 Road classes in terms of the geometric mean of the reference PSD

Road class	Roughness degree, $G_d(n_0)$ $(10^{-6}\ m^3)$
A	16
B	64
C	256
D	1024
E	4096
F	16,384
G	65,536
H	262,144

$$G_{dc}(f) = \gamma(f)\, G_d(f) = \gamma(f)\, G_d(f_0) \left(\frac{f}{f_0}\right)^{-w}, \tag{6}$$

in which $G_{dc}(f)$ is the vertical displacement cross-PSD imposed on the front left tire of the vehicle model, in m^2 s, and $\gamma(f)$ is a coherence function between the two PSDs.

According to Sekulic et al. (2013), $\gamma(f)$ is the square of a transfer function filter module for discrete frequencies of excitation, and it is defined by:

$$\gamma(f) = \frac{v_l^2}{v_l^2 + \left(\frac{f}{v}\right)^2}, \tag{7}$$

in which v_l is the cut-off frequency whose value (0.2 m^{-1}) was found by experimental measurements.

The road vertical displacement signals in the time domain can be generated from each of the corresponding vertical displacement PSDs through the method proposed by Shinozuka and Jan (1972). A compact formulation of this method is given by:

$$z(t) = \sum_{k=1}^{N} \sqrt{2\, G_d^*(f_k)\, \Delta f_k}\, \cos(2\pi f_k\, t + \psi_k), \tag{8}$$

in which $z(t)$ is the vertical displacement of the road in m, N is the number of intervals in the frequency domain, $G_d^*(f_k)$ is the road's vertical displacement PSD in m^2 s, Δf_k is the frequency resolution in Hz, and ψ_k is an independent random phase angle uniformly distributed between 0 and 2π rad. By replacing $G_d^*(f_k)$ with $G_d(f_k)$ and $G_{dc}(f_k)$, obtained through Eqs. (5) and (6), respectively, one can find, in the following order, $z_d(t)$ and $z_{dc}(t)$, which represent the vertical displacements imposed by the road profile on the front right and front left tires of the vehicle model. The differentiation of Eq. (8) provides vectors that represent the vertical velocities or accelerations of the road profile.

According to ISO 8608 (2016), it can be assumed that the rear tires experience the same imposed excitation as the front tires after a delay given by T, in s, defined by:

$$T = \frac{l}{v}, \tag{9}$$

in which l is the wheelbase of the vehicle model, in m.

Through the application of this delay in $z_d(t)$ and $z_{dc}(t)$, one can obtain $z_{dt}(t)$ and $z_{dcr}(t)$, which represent the vertical displacements, in m, imposed by the road profile on the rear right and rear left tires of the vehicle model, respectively.

2.2 Full-car model

An 8-DOF full-car model with passive suspension was used in this work. The model is composed of a seat, a sprung mass and four unsprung masses. The seat suspension, the tires and the suspension system are modelled with aggregated parameters representing linear springs and dampers. Figure 1 illustrates the full-car

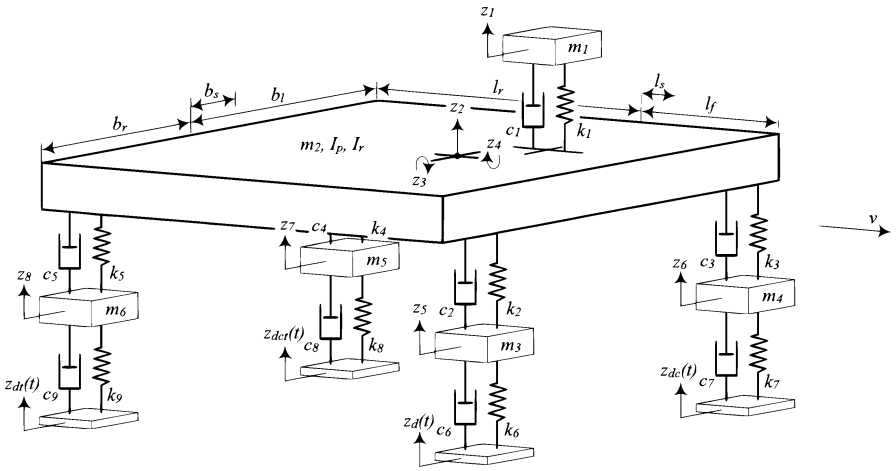

Fig. 1 Full-car model

model used here; the associated motion equation and matrices are given in Eqs. (10)–(15). Table 2 associates each DOF of the model with its variables and units.

$$\mathbf{M}\,\ddot{\mathbf{z}} + \mathbf{C}\,\dot{\mathbf{z}} + \mathbf{K}\,\mathbf{z} = \mathbf{P}, \tag{10}$$

$$\mathbf{M} = \begin{bmatrix} m_1 & 0 & 0 & 0 & 0 & 0 & 0 & 0 \\ & m_2 & 0 & 0 & 0 & 0 & 0 & 0 \\ & & I_p & 0 & 0 & 0 & 0 & 0 \\ & & & I_r & 0 & 0 & 0 & 0 \\ & & & & m_3 & 0 & 0 & 0 \\ & & & & & m_4 & 0 & 0 \\ & & & & & & m_5 & 0 \\ \text{sym.} & & & & & & & m_6 \end{bmatrix}, \tag{11}$$

$$\mathbf{C} = \begin{bmatrix} c_1 & -c_1 & c_1 l_s & c_1 b_s & 0 & 0 & 0 & 0 \\ & c_1 + c_2 + c_3 + c_4 + c_5 & -c_1 l_s - c_2 l_f - c_3 l_f + c_4 l_r + c_5 l_r & -c_1 b_s + c_2 b_r - c_3 b_l - c_4 b_l + c_5 b_r & -c_2 & -c_3 & -c_4 & -c_5 \\ & & c_1 l_s^2 + c_2 l_f^2 + c_3 l_f^2 + c_4 l_r^2 + c_5 l_r^2 & c_1 b_s l_s - c_2 b_r l_f + c_3 b_l l_f - c_4 b_l l_r + c_5 b_r l_r & c_2 l_f & c_3 l_f & -c_4 l_r & -c_5 l_r \\ & & & c_1 b_s^2 + c_2 b_r^2 + c_3 b_l^2 + c_4 b_l^2 + c_5 b_r^2 & -c_2 b_r & c_3 b_l & c_4 b_l & -c_5 b_r \\ & & & & c_2 + c_6 & 0 & 0 & 0 \\ & & & & & c_3 + c_7 & 0 & 0 \\ & & & & & & c_4 + c_8 & 0 \\ \text{sym.} & & & & & & & c_5 + c_9 \end{bmatrix}, \tag{12}$$

$$\mathbf{K} = \begin{bmatrix} k_1 & -k_1 & k_1 l_s & k_1 b_s & 0 & 0 & 0 & 0 \\ & k_1 + k_2 + k_3 + k_4 + k_5 & -k_1 l_s - k_2 l_f - k_3 l_f + k_4 l_r + k_5 l_r & -k_1 b_s + k_2 b_r - k_3 b_l - k_4 b_l + k_5 b_r & -k_2 & -k_3 & -k_4 & -k_5 \\ & & k_1 l_s^2 + k_2 l_f^2 + k_3 l_f^2 + k_4 l_r^2 + k_5 l_r^2 & k_1 b_s l_s - k_2 b_r l_f + k_3 b_l l_f - k_4 b_l l_r + k_5 b_r l_r & k_2 l_f & k_3 l_f & -k_4 l_r & -k_5 l_r \\ & & & k_1 b_s^2 + k_2 b_r^2 + k_3 b_l^2 + k_4 b_l^2 + k_5 b_r^2 & -k_2 b_r & k_3 b_l & k_4 b_l & -k_5 b_r \\ & & & & k_2 + k_6 & 0 & 0 & 0 \\ & & & & & k_3 + k_7 & 0 & 0 \\ & & & & & & k_4 + k_8 & 0 \\ \text{sym.} & & & & & & & k_5 + k_9 \end{bmatrix}, \tag{13}$$

Table 2 Variables of each degree of freedom of the full-car model

Variable	Degree of freedom
z_1	Driver seat vertical displacement (m)
z_2	Body vertical displacement (m)
z_3	Body pitch angular displacement (rad)
z_4	Body roll angular displacement (rad)
z_5	Front right wheel vertical displacement (m)
z_6	Front left wheel vertical displacement (m)
z_7	Rear left wheel vertical displacement (m)
z_8	Rear right wheel vertical displacement (m)

$$\mathbf{P} = \begin{bmatrix} 0 & 0 & 0 & 0 & k_6 z_d + c_6 \dot{z}_d & k_7 z_{dc} + c_7 \dot{z}_{dc} & k_8 z_{dct} + c_8 \dot{z}_{dct} & k_9 z_{dt} + c_9 \dot{z}_{dt} \end{bmatrix}^T, \tag{14}$$

$$\mathbf{z} = \begin{bmatrix} z_1 & z_2 & z_3 & z_4 & z_5 & z_6 & z_7 & z_8 \end{bmatrix}^T. \tag{15}$$

2.3 Optimization of systems

Optimization methods are basically divided into two classes: deterministic and stochastic. Deterministic approaches produce the same steps towards the solution when initiating the procedure from the same starting point, and stochastic approaches do not.

In some optimization problems, more than one objective function must be minimized or maximized. These are multi-objective optimization problems, which seek a set of design variables, or a design vector, that satisfies more than one objective function simultaneously.

In optimization problems with conflicting objective functions, the solution of the problem converges to an array of design vectors. The optimal set of design vectors is called the Pareto-optimal front, and it provides a group of optimal solutions from which the designer can select the best one for the specific situation. This group of optimal solutions contains design vectors that minimize or maximize each of the objective functions individually, as well as ones that provide intermediate solutions, weighting each objective function differently.

A multi-objective optimization problem can be mathematically defined as follows:

$$\min \mathbf{F}(\mathbf{x}) = [F_1(\mathbf{x}), F_2(\mathbf{x}), \ldots, F_k(\mathbf{x})]^T, \tag{16}$$

subject to:

$$\begin{aligned} g_i(\mathbf{x}) &\leq 0\ ,\ i = 1, 2, \ldots, p, \\ h_j(\mathbf{x}) &= 0\ ,\ j = 1, 2, \ldots, q, \\ x_{i,lb} &\leq x_i \leq x_{i,ub}\ ,\ i = 1, 2, \ldots, n, \end{aligned} \tag{17}$$

in which $\mathbf{x} = [x_1, x_2, \ldots, x_n]$ is the design vector, $\mathbf{F}(\mathbf{x}) \in \Re^k$ is the objective function vector, $g_i(\mathbf{x})$ are the inequality constraints, $h_j(\mathbf{x})$ are the equality constraints, $x_{i,lb}$ are the design variable lower bounds, $x_{i,ub}$ are the design variable upper bounds, and k, p, q and n are the number of objective functions, inequality constraints, equality constraints and design variables, respectively.

Metaheuristic approaches, according to Bianchi et al. (2009), are capable of finding good solutions to optimization problems with a realistic search-space. According to Miguel and Fadel Miguel (2012) and Fadel Miguel et al. (2013), the advantages of these algorithms include: (1) they do not require gradient information and can be applied to problems in which the gradient is difficult to obtain or simply does not exist; (2) they do not become stuck in local minima if correctly tuned; (3) they can be applied to non-smooth or discontinuous functions; (4) they furnish a set of optimal solutions instead of a single solution, giving the designer a set of options from which to choose; and (5) they can be used to solve mixed-variable optimization problems. Some algorithms stand out among the wide variety of metaheuristic algorithms in the literature: the Genetic Algorithm (Holland 1975), the Krill Herd Algorithm (Gandomi et al. 2013), Particle Swarm Optimization (Eberhart and Kennedy 1995), Harmony Search (Geem et al. 2001), the Firefly Algorithm (Yang 2010), and Cuckoo Search (Yang and Deb 2010).

The methodology proposed here uses NSGA-II, a multi-objective metaheuristic algorithm developed by Deb et al. (2002) based on the genetic algorithm. Gadhvi et al. (2016) state that some of the many multi-objective optimization algorithms have received much attention in science, engineering and business applications because of their ability to obtain the Pareto front closest to the true Pareto front, and NSGA-II is one of the most relevant algorithms.

2.4 Vehicle comfort and safety

The ISO 2631-1 (1997) standard suggests that for some environments it is possible to evaluate the effects of vibration on human comfort by using the frequency-weighted RMS acceleration of a representative time interval, weighted according to a given weighting curve. Six subjective comfort ranges are proposed by the standard, as shown in Table 3.

Vehicle safety involves several different concepts. Tire grip is directly related to the stability and therefore the safety of the vehicle. A better adherence to the track occurs when the vehicle's tires are in contact with the road surface at all times, i.e., the dynamic loads acting on the wheels do not exceed the static loads due to the vehicle's weight. To ensure this, the relative dynamic loading must be less than one at all times in every wheel. Wang et al. (2010) explain that reducing these factors ensures a lower vibration of the vehicle's wheels, which translates into a lower

Table 3 Comfort as a function of the weighted RMS accelerations imposed on the human body

Weighted RMS acceleration	Probable sensation
Less than 0.315 m/s^2	Not uncomfortable
0.315–0.63 m/s^2	Slightly uncomfortable
0.5–1 m/s^2	Fairly uncomfortable
0.8–1.6 m/s^2	Uncomfortable
1.25–2.5 m/s^2	Very uncomfortable
Greater than 2 m/s^2	Extremely uncomfortable

impact transmission from the road irregularities to the tires and hence to the sprung masses.

Finally, an observation should be made on the suspension stroke, a vehicle design parameter that affects both comfort and safety. Vehicles must be designed to accommodate a suspension system that absorbs vibration imposed by road irregularities without bumping into the suspension stoppers, possibly causing undesirable noise and vibration to the passengers or even the premature failure of the suspension components. According to Gillespie (2010), most large cars have a usable suspension stroke in the range of 177.8–203.2 mm, while for compact cars the stroke varies between 127 and 152.4 mm.

3 Proposed multi-objective optimization of a vehicle suspension

We carry out the multi-objective optimization of the aggregated parameters of the passive suspension system of a full-car model. We use NSGA-II for this optimization, which requires a multi-objective approach, since the main objectives conflict.

One of the main objectives of the vehicle's suspension system is associated with passenger comfort, which is influenced by the seat motion and absorbed by the body of the passengers. Another important objective relates to safety, which is affected by the tire grip of the road surface. Lastly, a third objective is related to the trade-off of providing desirable levels of comfort and safety with the smallest possible suspension stroke. These are the three objective functions of the optimization problem.

The basic structure of the proposed routine is illustrated by the flowchart in Fig. 2, which, along with Table 4, shows each step of the algorithm and how they interact. We detail each step below.

3.1 Multiple-track roughness simulation

The vehicle model in our study is considered to travel at a constant speed, v, of 20 m/s over an ISO 8608 (2016) class C road profile, considered to be of intermediate roughness. As stated by Ngwangwa et al. (2014), this class is representative of a damaged pavement with frequent shallow depressions, some

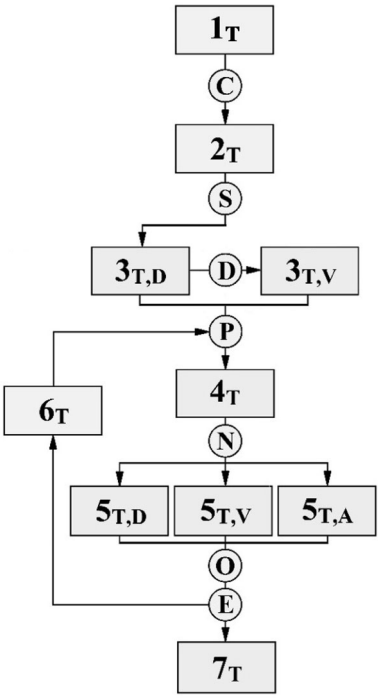

Fig. 2 Basic flowchart of the computational routine

deep, or a maintained unpaved road. According to Dodds and Robson (1973), this class represents a principal road in a poor state of repair.

By associating Eqs. (1)–(7), it is possible to obtain expressions for the vertical displacement PSD and cross-PSD, in terms of temporal frequency, imposed on the front right and front left tires of the full-car model. Following the ISO 8608 (2016) guidelines, it is considered that the temporal frequency ranges between 0.22 and 56.6 Hz, with a resolution, Δf, of 0.02 Hz, in order to avoid spectral leakage in frequencies near 0 Hz.

The vertical displacements imposed by the road profile on the front right and front left tires can be obtained by combining Eqs. (5)–(8). The differentiation of the resulting expressions provides the vertical velocities imposed on the tires of the vehicle. A time range of 50 s ($0 \leq t \leq 50$ s) with a resolution of 0.01 s was chosen. The delay between the excitation of the front and rear tires of the vehicle model, calculated by Eq. (9), is 0.13 s.

3.2 Mechanical and geometric parameters of the full-car model

The mechanical and geometric parameters of the vehicle model used in this work are based on Xie et al. (2013) and described in Table 5.

Due to the longitudinal symmetry of the vehicle model, the ten design variables shown in Table 5 are reduced to six and the design vector is:

Table 4 Description of each step of the computational routine

		Step description
Step nomenclature in the flowchart	1_T	Vertical displacement PSD from ISO 8608 (2016) class C road profile
	C	Cross-PSD computation
	2_T	PSD and cross-PSD of the vertical displacements and velocities imposed on the front tires of the vehicle model
	S	Digital simulation of the temporal signals associated with the PSDs by the method proposed by Shinozuka and Jan (1972)
	$3_{T,D}$	Vertical displacements imposed by the road on each of the vehicle model tires
	D	Numerical differentiation using the finite difference method
	$3_{T,V}$	Vertical velocities imposed by the road on each of the vehicle model tires
	P	Design vector and input data of the optimization problem
	4_T	Full-car model
	N	Numerical integration of the equation of motion using the Newmark method
	$5_{T,D}$	Dynamic behavior of the vehicle model in terms of displacements
	$5_{T,V}$	Dynamic behavior of the vehicle model in terms of velocities
	$5_{T,A}$	Dynamic behavior of the vehicle model in terms of accelerations
	O	Objective function vector computation
	E	Stopping criterion
	6_T	NSGA-II multi-objective optimization algorithm proposed by Deb et al. (2002)
	7_T	Pareto-optimal front obtained through the multi-objective optimization process

$$\mathbf{x} = [\,x_1 \quad x_2 \quad x_3 \quad x_4 \quad x_5 \quad x_6\,]^T = [\,k_1 \quad c_1 \quad k_2 \quad c_2 \quad k_4 \quad c_4\,]^T. \tag{18}$$

These are the six parameters that are modified at each generation of the optimization procedure. Wang et al. (2010), Xie et al. (2013), Meng et al. (2014) and Song et al. (2014) use reference values for each of these parameters. Thereby, a full-car model with a non-optimized suspension system can be completely defined for further comparison purposes.

The design vector composed of the reference parameters, represented by $\mathbf{x}_R$, is called the reference design vector and has the values given in Table 6.

3.3 Dynamic analysis

The numerical integration of the motion equation of the vehicle model can be performed through the Newmark method. This integration allows the assessment of the dynamic behavior of the eight DOFs of the model in terms of vertical

Table 5 Mechanical and geometric parameters of the full-car model used in this work

Parameter	Description	Value
k_i	Driver seat (i = 1), front right (i = 2), front left (i = 3), rear left (i = 4) and rear right (i = 5) spring stiffness coefficients	Design variables
k_j	Front right (j = 1), front left (j = 2), rear left (j = 3) and rear right (j = 4) tire stiffness coefficients	250 kN/m
c_i	Driver seat (i = 1), front right (i = 2), front left (i = 3), rear left (i = 4) and rear right (i = 5) damper damping coefficients	Design variables
c_j	Front right (j = 1), front left (j = 2), rear left (j = 3) and rear right (j = 4) tire damping coefficients	150 N s/m
m_1	Seat and driver mass	90 kg
m_2	Sprung mass	1100 kg
I_p	Pitch moment of inertia	1848 kg m^2
I_r	Roll moment of inertia	550 kg m^2
m_i	Front right (i = 3) and front left (i = 4) wheel masses	25 kg
m_j	Rear left (j = 5) and rear right (j = 6) wheel masses	45 kg
l_s	Longitudinal distance between the driver seat and the sprung mass center of gravity	0.3 m
l_f	Longitudinal distance between the front axle and the sprung mass center of gravity	1.2 m
l_r	Longitudinal distance between the rear axle and the sprung mass center of gravity	1.4 m
b_s	Transversal distance between the driver seat and the sprung mass center of gravity	0.25 m
b_l	Transversal distance between the left wheels and the sprung mass center of gravity	1.0 m
b_r	Transversal distance between the right wheels and the sprung mass center of gravity	0.25 m

Table 6 Reference values of the parameters that form the reference design vector, $\mathbf{x}_R$

Design variable	Description	Reference value
k_1	Driver seat stiffness coefficient	15 kN/m
$k_2 = k_3$	Front springs stiffness coefficient	15 kN/m
$k_4 = k_5$	Rear springs stiffness coefficient	17 kN/m
c_1	Driver seat damping coefficient	150 N s/m
$c_2 = c_3$	Front dampers damping coefficient	2.5 kN s/m
$c_4 = c_5$	Rear dampers damping coefficient	2.5 kN s/m

displacements, velocities and accelerations, represented, respectively, by $\mathbf{z}(t)$, in m, $\dot{\mathbf{z}}(t)$, in m/s and $\ddot{\mathbf{z}}(t)$, in m/s^2. These vectors form a set of 24 temporal signals, which are obtained at each execution of the dynamic analysis.

It is, then, possible to calculate, using Eqs. (19)–(21), the RMS values of the vertical displacements, RMS($\mathbf{z}$), in m, velocities, RMS($\dot{\mathbf{z}}$), in m/s, and accelerations, RMS($\ddot{\mathbf{z}}$), in m/s^2, of the eight DOFs of the vehicle model.

$$\mathrm{RMS}(\mathbf{z}) = \left[\frac{1}{T}\int_0^{\infty} \mathbf{z}(t)^2 dt\right]^{\frac{1}{2}}, \tag{19}$$

$$\mathrm{RMS}(\dot{\mathbf{z}}) = \left[\frac{1}{T}\int_0^{\infty} \dot{\mathbf{z}}(t)^2 dt\right]^{\frac{1}{2}}, \tag{20}$$

$$\mathrm{RMS}(\ddot{\mathbf{z}}) = \left[\frac{1}{T}\int_0^{\infty} \ddot{\mathbf{z}}(t)^2 dt\right]^{\frac{1}{2}}. \tag{21}$$

3.4 Optimization procedure

The mathematical formulation of the multi-objective optimization problem is given in Eqs. (22)–(44). The problem consists in minimizing the objective vector:

$$\min \mathbf{F_T}(\mathbf{x}) = [F_{T1}(\mathbf{x}),\, F_{T2}(\mathbf{x}),\, F_{T3}(\mathbf{x})]^T, \tag{22}$$

where $\mathbf{F_T}(\mathbf{x})$ is the objective vector, which is composed of the weighted RMS value of the driver's seat vertical acceleration, $F_{T1}(\mathbf{x})$, in m/s^2; the mean RMS value of the model wheels' dynamic amplification factor, $F_{T2}(\mathbf{x})$, dimensionless, and the maximum relative displacement between each wheel and the body of the vehicle model, $F_{T3}(\mathbf{x})$, in mm.

Considering the design vector, $\mathbf{x}$, given in Eq. (18), the first objective function, $F_{T1}(\mathbf{x})$, in m/s^2, can be defined by:

$$F_{T1}(\mathbf{x}) = \left\{\sum_i \left[W_i\, \mathrm{RMS}(\ddot{z}_1)_i\right]^2\right\}^{\frac{1}{2}}, \tag{23}$$

in which W_i and $\mathrm{RMS}(\ddot{z}_1)_i$ are, respectively, the weighting factor and the RMS value of the driver's seat vertical acceleration for the ith one-third octave band, according to the ISO 2631-1 (1997) standard.

Figure 3 illustrates, using the weighting factors and the one-third octave bands provided by ISO 2631-1 (1997), the standard frequency weighting curve for the vertical motions imposed on the human body in the vertical recumbent direction (except the head).

Griffin (1990) explains that the RMS value of the driver's seat vertical acceleration for the ith one-third octave band can be obtained via:

$$\mathrm{RMS}(\ddot{z}_1)_i = (\Delta f\, G_{A1Ti})^{\frac{1}{2}}, \tag{24}$$

where G_{A1Ti} is the driver's seat vertical acceleration PSD for the ith one-third octave band, in m^2 s, obtained from the time history of the driver seat vertical acceleration.

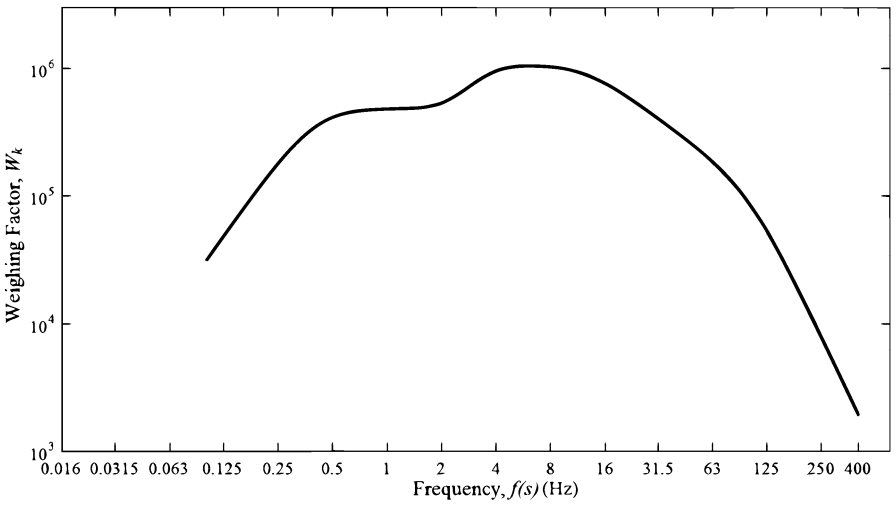

Fig. 3 Frequency weighting curve for the vertical motions imposed on the human body in the vertical recumbent direction (except the head)

The second objective function, $F_{T2}(\mathbf{x})$, consists in the mean RMS value of the model wheels' dynamic amplification factor. These factors are dimensionless, and the expression that represents this objective function, as well as those related to it, is as follows:

$$F_{T2}(\mathbf{x}) = \left\{ \frac{1}{T} \int_0^T \left[\frac{\frac{F_{d1}(t)}{G_1} + \frac{F_{d2}(t)}{G_2} + \frac{F_{d3}(t)}{G_3} + \frac{F_{d4}(t)}{G_4}}{4} \right]^2 dt \right\}^{\frac{1}{2}}, \tag{25}$$

where $F_{d1}(t)$, $F_{d2}(t)$, $F_{d3}(t)$ and $F_{d4}(t)$ are the dynamic loads, in N, acting, respectively, on the front right, front left, rear left and rear right wheels of the vehicle model, defined in Eqs. (26)–(29); and G_1, G_2, G_3 and G_4 are the static loads, in N, acting, in the same order, on the wheels of the vehicle model, defined in Eqs. (30)–(33).

$$F_{d1}(t) = c_2 \left(\dot{z}_5 - \dot{z}_2 + l_f \dot{z}_3 - b_r \dot{z}_4 \right) + k_2 \left(z_5 - z_2 + l_f z_3 - b_r z_4 \right) + m_3 \ddot{z}_5, \tag{26}$$

$$F_{d2}(t) = c_3 \left(\dot{z}_6 - \dot{z}_2 + l_f \dot{z}_3 + b_l \dot{z}_4 \right) + k_3 \left(z_6 - z_2 + l_f z_3 + b_l z_4 \right) + m_4 \ddot{z}_6, \tag{27}$$

$$F_{d3}(t) = c_4 \left(\dot{z}_7 - \dot{z}_2 - l_r \dot{z}_3 + b_l \dot{z}_4 \right) + k_4 \left(z_7 - z_2 - l_r z_3 + b_l z_4 \right) + m_5 \ddot{z}_7, \tag{28}$$

$$F_{d4}(t) = c_5 \left(\dot{z}_8 - \dot{z}_2 - l_r \dot{z}_3 - b_r \dot{z}_4 \right) + k_5 \left(z_8 - z_2 - l_r z_3 - b_r z_4 \right) + m_6 \ddot{z}_8, \tag{29}$$

$$G_1 = m_2 \, g \, \frac{l_r}{l_f + l_r} \, \frac{b_l}{b_l + b_r}, \tag{30}$$

$$G_2 = m_2\, g\, \frac{l_r}{l_f + l_r}\, \frac{b_r}{b_l + b_r}, \tag{31}$$

$$G_3 = m_2\, g\, \frac{l_f}{l_f + l_r}\, \frac{b_r}{b_l + b_r}, \tag{32}$$

$$G_4 = m_2\, g\, \frac{l_f}{l_f + l_r}\, \frac{b_l}{b_l + b_r}, \tag{33}$$

in which g is the acceleration of gravity, equal to $-\ 9.807\ \mathrm{m/s^2}$.

It is important to note that the masses of the wheels, seat and driver were neglected in the static load calculation, since they have much smaller values than the sprung mass.

The third and last objective function, $F_{T3}(\mathbf{x})$, in mm, is as follows:

$$F_{T3}(\mathbf{x}) = 10^3 \left\{ \max_{i \in [1,2,3,4]} \left\{ \max_{t \in [0,T]} [f_{di}(t)] \right\} \right\}, \tag{34}$$

where $f_{d1}(t), f_{d2}(t), f_{d3}(t)$ and $f_{d4}(t)$ are, respectively, the relative displacements, in mm, between the body and the front right, front left, rear left and rear right wheels of the vehicle, defined in Eqs. (35)–(38).

$$f_{d1}(t) = z_2 - l_f z_3 + b_r z_4 - z_5, \tag{35}$$

$$f_{d2}(t) = z_2 - l_f z_3 - b_l z_4 - z_6, \tag{36}$$

$$f_{d3}(t) = z_2 + l_r z_3 - b_l z_4 - z_7, \tag{37}$$

$$f_{d4}(t) = z_2 + l_r z_3 + b_r z_4 - z_8. \tag{38}$$

There are no equality or inequality constraints in the formulation. The design variables are assumed to be continuous and have the ranges given in Eqs. (39)–(44), which are identical to those used by Wang et al. (2010), Xie et al. (2013), Meng et al. (2014) and Song et al. (2014).

$$7500\ \mathrm{N/m} \leq x_1 \leq 22500\ \mathrm{N/m}, \tag{39}$$

$$75\ \mathrm{N\,s/m} \leq x_2 \leq 225\ \mathrm{N\,s/m}, \tag{40}$$

$$7500\ \mathrm{N/m} \leq x_3 \leq 22500\ \mathrm{N/m}, \tag{41}$$

$$1250\ \mathrm{N\,s/m} \leq x_4 \leq 3750\ \mathrm{N\,s/m}, \tag{42}$$

$$8500\ \mathrm{N/m} \leq x_5 \leq 22500\ \mathrm{N/m}, \tag{43}$$

$$1250\ \mathrm{N\,s/m} \leq x_6 \leq 3750\ \mathrm{N\,s/m}. \tag{44}$$

The solution of the multi-objective optimization problem defined above follows the sequence of the flowchart presented in Fig. 2. With the definition of the

Table 7 Stopping criteria and additional parameters used in the execution of NSGA-II

Design variables	6	Pareto fraction	1
Population size	20	Objective function evaluation	Parallel
		Stopping criteria	
Creation function	Uniform	Generations	30
Selection	Tournament	Time	∞
Crossover function	Intermediate	Fitness limit	$-\infty$
Mutation function	Gaussian	Objective function tolerance	10^{-3}
Crossover probability	80%	Maximum stalled generations	10
Mutation probability	20%	Maximum stalled time	∞

objective vector, the design vector and the ranges of the design variables, the optimization algorithm is executed until one of the stopping criteria is satisfied. The stopping criteria, as well as additional parameters used in the execution, are given in Table 7.

4 Numerical results

This section gives our numerical results. The results obtained in the modal and dynamic analysis of the full-car model with optimized and non-optimized suspension systems are also presented and discussed.

4.1 Reference dynamic behavior

The mean value and variance of the RMS values of 50 executions of the dynamic analyses of our vehicle model are used to present its dynamic behavior and objective function values. Tables 8 and 9 give these results, obtained using the reference design vector, $\mathbf{x}_{\boldsymbol{R}}$. The number of executions was chosen by conducting a convergence study of these statistical measures.

Table 8 Mean values and variances of the vertical displacements, velocities and accelerations RMS values (reference design vector)

	$\mu[\text{RMS}(\mathbf{z})]$	$\text{var}[\text{RMS}(\mathbf{z})]$		$\mu[\text{RMS}(\dot{\mathbf{z}})]$	$\text{var}[\text{RMS}(\dot{\mathbf{z}})]$		$\mu[\text{RMS}(\ddot{\mathbf{z}})]$	$\text{var}[\text{RMS}(\ddot{\mathbf{z}})]$
z_1	0.0142	4.4321E−07	$\dot{z}_1$	0.0866	9.3235E−06	$\ddot{z}_1$	0.9052	1.6843E−03
z_2	0.0127	3.6762E−07	$\dot{z}_2$	0.0516	1.7247E−06	$\ddot{z}_2$	0.7841	7.5655E−05
z_3	0.0023	5.1706E−09	$\dot{z}_3$	0.0254	4.5087E−07	$\ddot{z}_3$	0.6421	6.3386E−05
z_4	0.0151	9.5635E−07	$\dot{z}_4$	0.0648	3.9763E−06	$\ddot{z}_4$	0.9637	2.1434E−04
z_5	0.0158	1.0939E−10	$\dot{z}_5$	0.2174	6.4956E−09	$\ddot{z}_5$	20.4292	4.4383E−06
z_6	0.0152	1.1062E−10	$\dot{z}_6$	0.1102	2.8576E−08	$\ddot{z}_6$	4.9559	8.9259E−05
z_7	0.0151	1.2003E−10	$\dot{z}_7$	0.1155	3.1714E−08	$\ddot{z}_7$	4.8270	1.4759E−04
z_8	0.0159	1.5907E−10	$\dot{z}_8$	0.2171	1.8655E−08	$\ddot{z}_8$	15.6796	1.9670E−05

Table 9 Mean values and variances of the objective vector components (reference design vector)

	$\mu[F_T(\mathbf{x}_R)]$	$\text{var}[F_T(\mathbf{x}_R)]$
$F_1(\mathbf{x}_R)$ (m/s^2)	0.2625	1.73E−03
$F_2(\mathbf{x}_R)$	0.1811	2.74E−06
$F_3(\mathbf{x}_R)$ (mm)	32.8665	12.542

Table 10 Natural frequencies of the vehicle model (reference design vector)

Natural frequencies, f_{nn} (Hz)							
f_{n1}	0.9759	f_{n3}	1.3969	f_{n5}	12.2615	f_{n7}	16.3872
f_{n2}	1.1833	f_{n4}	2.2027	f_{n6}	12.2644	f_{n8}	16.3886

The modal analysis is presented in Tables 10 and 11, which show, respectively, the natural frequencies and the modes of vibration of the vehicle model with the non-optimized suspension system.

Analyzing Tables 10 and 11, it can be verified that the first four modes of vibration are associated with natural frequencies in the range of 0.9759 and 2.2027 Hz, and mainly excite one or more DOFs of the sprung masses. The excitation of the unsprung masses, however, is associated with the remaining four DOFs, which are related to natural frequencies ranging between 12.2615 and 16.3886 Hz. The DOFs associated with the motions of the unsprung masses are poorly excited in the first four modes of vibration of the vehicle model. Similarly, there is a low excitation of the DOFs related to the motion of the sprung masses in the fifth to eighth modes of vibration of the model.

4.2 Optimization of the suspension system of the full-car model

The Pareto-optimal front is used to give the values of the design variables and objective functions of four optimal design vectors, called the design vectors of interest. These vectors are those that minimize each of the objective functions, F_{T1}, F_{T2} and F_{T3}, individually, denoted $\mathbf{x}_{T1}$, $\mathbf{x}_{T2}$ and $\mathbf{x}_{T3}$, respectively; and also the vector that provides the solution chosen as ideally weighted between the comfort and safety of the vehicle model for the present analysis, called the weighted design vector and denoted $\mathbf{x}_{TP}$.

We emphasize the versatility of the Pareto-optimal front in providing a set of non-dominated solutions that allows the designer to choose the one most appropriate for the real problem. The selection of the weighted design vector illustrates this decision process, assuming that the optimized suspension system must provide the highest possible comfort to the passengers without compromising their safety.

Using the parameters and stopping criteria of Table 7, the execution of the multi-objective optimization algorithm yields the Pareto-optimal front given in Fig. 4. Table 12 gives the value of each variable in the design vectors of interest, as well as the values of the objective functions generated by these vectors.

According to the ISO 2631-1 (1997) standard, there is no discomfort for the driver in the cases in which the weighted RMS value of the driver's seat vertical

Table 11 Modes of vibration associated with each natural frequency of the vehicle model (reference design vector)

		Modes of vibration, $\mathbf{C}_n$							
		$\mathbf{C}_1$	$\mathbf{C}_2$	$\mathbf{C}_3$	$\mathbf{C}_4$	$\mathbf{C}_5$	$\mathbf{C}_6$	$\mathbf{C}_7$	$\mathbf{C}_8$
Degrees of freedom	z_1	2.776E−2	− 1.002E−2	3.548E−2	− 9.477E−2	1.827E−6	− 1.524E−5	7.045E−7	− 8.112E−6
	z_2	2.416E−2	3.989E−3	1.320E−2	1.160E−2	1.558E−4	5.343E−4	− 1.286E−4	3.430E−4
	z_3	− 6.951E−3	2.079E−2	7.634E−3	− 1.376E−3	1.311E−4	4.432E−4	9.241E−5	− 2.442E−4
	z_4	1.901E−2	1.778E−2	− 3.266E−2	− 8.535E−3	7.189E−4	− 5.060E−4	− 4.490E−4	− 3.667E−4
	z_5	2.386E−3	− 6.868E−4	− 7.004E−4	5.177E−4	4.604E−5	− 3.225E−5	1.823E−1	− 8.228E−2
	z_6	7.663E−4	− 2.205E−3	2.093E−3	1.256E−3	− 9.266E−5	6.545E−5	− 8.228E−2	− 1.823E−1
	z_7	− 2.937E−4	9.843E−4	3.648E−3	1.198E−3	7.112E−2	− 1.310E−1	− 3.640E−5	− 2.976E−5
	z_8	1.534E−3	2.699E−3	4.880E−4	3.556E−4	− 1.310E−1	− 7.110E−2	1.811E−5	1.474E−5

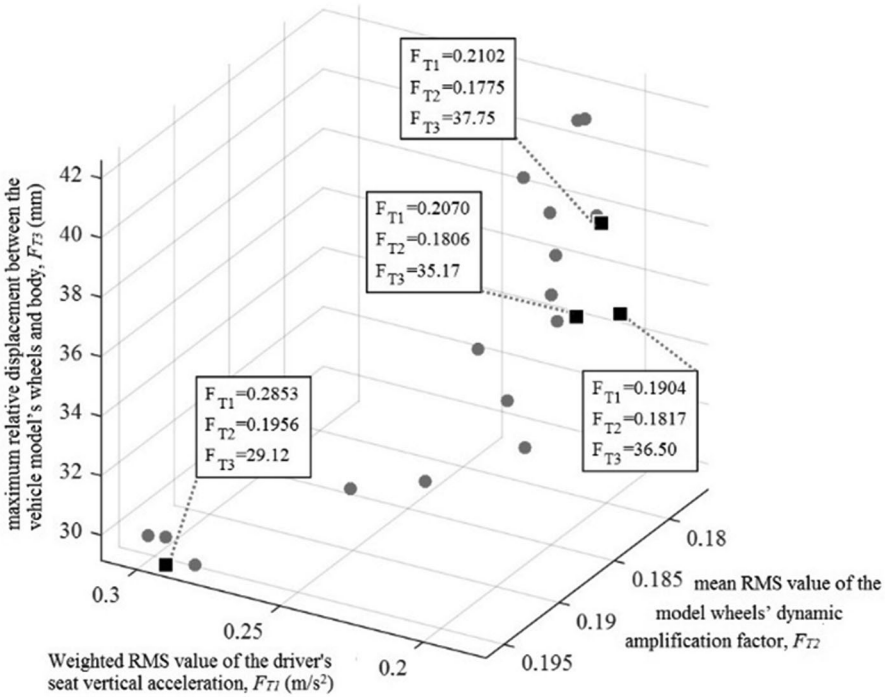

Fig. 4 Pareto-optimal front and solutions generated by the design vectors of interest

Table 12 Design variables in the design vectors of interest and objective functions generated by these vectors

	k_1 (N/m)	c_1 (Ns/m)	k_2, k_3 (N/m)	c_2, c_3 (Ns/m)	k_4, k_5 (N/m)	c_4, c_5 (Ns/m)	F_{T1} (m/s^2)	F_{T2}	F_{T3} (mm)
$\mathbf{x}_{T1}$	8093.53	131.23	7630.39	2179.14	12,132.24	1639.83	0.1904	0.1817	36.50
$\mathbf{x}_{T2}$	10,208.91	162.97	8615.32	1907.65	17,808.98	2048.16	0.2102	0.1775	37.75
$\mathbf{x}_{T3}$	15,506.67	110.17	13,630.94	3329.68	17,518.83	3365.77	0.2853	0.1956	29.12
$\mathbf{x}_{TP}$	8094.40	121.94	9286.10	2309.71	13,450.06	1946.15	0.2070	0.1806	35.17

accelerations is lower than 0.315 m/s^2. Thus, the weighted design vector is chosen to be the one that generates a solution in which the first objective function, F_{T1}, is the lowest within this range, as long as the value of the second objective function, F_{T2}, is at least kept constant with respect to the reference value. To prevent the losing of contact between the tires and the road, the dynamic amplification factors of each wheel of the vehicle model must be less than one at all times. Similarly, this compromise is ensured by maintaining F_{T3} below the 127 mm limit, in such a way that even with the smallest suspension stroke usually found in compact cars,

Table 13 Natural frequencies of the vehicle model (weighted design vector)

Natural frequencies, f_{nn} (Hz)							
f_{n1}	0.7938	f_{n3}	1.2031	f_{n5}	12.1790	f_{n7}	16.2089
f_{n2}	1.0088	f_{n4}	1.6404	f_{n6}	12.1808	f_{n8}	16.2094

according to Gillespie (2010), the shock against the suspension stoppers does not occur.

4.3 Optimized dynamic behavior

The natural frequencies and the modes of vibration of the vehicle model with an optimized suspension system are given in Tables 13 and 14.

By comparing Tables 10 and 13, as well as Tables 11 and 14, it is possible to perceive a considerable reduction of the natural frequencies with the optimization of the suspension system of the vehicle model, maintaining similar modes of vibration. This reduction occurs especially on the natural frequencies related to the first four modes of vibration, which mainly excite one or more DOFs related to the sprung masses of the model. These frequencies decreased between 13.9 and 25.5%, while the remaining ones decreased between 0.7 and 1.1%.

The mean RMS values of the dynamic behavior of the vehicle models whose suspension systems use the design variables of both the reference and the weighted design vectors are shown in Tables 15 and 16, considering the 50 executions of the dynamic analysis.

The assessment of Tables 15 and 16 allows the recognition of some important changes resulting from the optimization of the suspension system. These changes are symbolized, in Table 16, by dots and arrows according to their value modification. The mean RMS values of the vertical or angular displacements remain virtually unchanged. The vertical or angular velocities, however, experience larger variations, decreasing between 9.5 and 14.6% in the sprung masses and increasing between 3.8 and 19.7% in the unsprung masses. The mean RMS values of the vertical or angular accelerations have the most significant modifications. The DOFs associated with the sprung masses reduced from 14.4 to 31.7%, while those associated with the unsprung masses increased from 10.2 to 25.6%.

These changes demonstrate a higher vibration absorption efficiency of the optimized suspension system compared to the non-optimized one. This evidences a lower velocity and acceleration transmissibility from the road to the sprung masses of the vehicle model with the optimized system.

Figures 5, 6 and 7 show the time histories of the functions associated with each objective function, considering both the parameters of the reference, $\mathbf{x}_{\boldsymbol{R}}$, and the weighted design vectors, $\mathbf{x}_{\boldsymbol{TP}}$. The mean RMS values of each objective function of the optimization problem, and the differences between them, are given in Table 17.

Analyzing Table 17 and Figs. 5, 6 and 7, we see that the first objective function decreased from 0.2625 to 0.2070 m/s^2 with the suspension system optimization, a substantial reduction of 21.14%. The second objective function decreased from 0.1811 to 0.1806, a 0.28% reduction that occurred without noticeable modifications

Table 14 Modes of vibration associated with each natural frequency of the vehicle model (weighted design vector)

		Modes of vibration, $\mathbf{C}_n$							
		$\mathbf{C}_1$	$\mathbf{C}_2$	$\mathbf{C}_3$	$\mathbf{C}_4$	$\mathbf{C}_5$	$\mathbf{C}_6$	$\mathbf{C}_7$	$\mathbf{C}_8$
Degrees of freedom	z_1	3.136E−2	− 1.140E−2	4.340E−2	− 9.008E−2	7.868E−7	− 6.572E−6	2.436E−7	− 8.112E−6
	z_2	2.338E−2	5.567E−3	1.234E−2	1.338E−2	1.248E−4	4.270E−4	− 8.128E−5	3.430E−4
	z_3	− 1.009E−2	1.756E−2	1.144E−2	− 2.260E−4	1.046E−4	3.549E−4	5.833E−5	− 2.442E−4
	z_4	1.489E−2	2.643E−2	− 2.766E−2	− 1.149E−2	5.752E−4	− 4.035E−4	− 2.837E−4	− 3.667E−4
	z_5	1.541E−3	− 8.221E−5	− 5.481E−4	2.860E−4	2.359E−5	− 1.651E−5	1.823E−1	− 8.228E−2
	z_6	7.397E−4	− 1.508E−3	9.463E−4	9.097E−4	− 4.738E−5	3.330E−5	− 8.235E−2	− 1.823E−1
	z_7	− 2.888E−4	1.911E−4	2.888E−3	1.277E−3	7.123E−2	− 1.309E−1	− 1.880E−5	− 2.976E−5
	z_8	8.560E−4	2.229E−3	7.484E−4	3.805E−4	− 1.309E−1	− 7.122E−2	9.361E−6	1.474E−5

Table 15 Mean RMS values of the vertical displacements, velocities and accelerations of the vehicle model (reference design vector)

RMS($\mathbf{z}$)		RMS($\dot{\mathbf{z}}$)		RMS($\ddot{\mathbf{z}}$)	
z_1 (m)	0.0142	$\dot{z}_1$ (m/s)	0.0866	$\ddot{z}_1$ (m/s^2)	0.9052
z_2 (m)	0.0127	$\dot{z}_2$ (m/s)	0.0516	$\ddot{z}_2$ (m/s^2)	0.7841
z_3 (rad)	0.0023	$\dot{z}_3$ (rad/s)	0.0254	$\ddot{z}_3$ (rad/s^2)	0.6421
z_4 (rad)	0.0151	$\dot{z}_4$ (rad/s)	0.0648	$\ddot{z}_4$ (rad/s^2)	0.9637
z_5 (m)	0.0158	$\dot{z}_5$ (m/s)	0.2174	$\ddot{z}_5$ (m/s^2)	20.4292
z_6 (m)	0.0152	$\dot{z}_6$ (m/s)	0.1102	$\ddot{z}_6$ (m/s^2)	4.9559
z_7 (m)	0.0151	$\dot{z}_7$ (m/s)	0.1155	$\ddot{z}_7$ (m/s^2)	4.8270
z_8 (m)	0.0159	$\dot{z}_8$ (m/s)	0.2171	$\ddot{z}_8$ (m/s^2)	15.6796

Table 16 Mean RMS values of the vertical displacements, velocities and accelerations of the vehicle model (weighted design vector)

RMS($\mathbf{z}$)		RMS($\dot{\mathbf{z}}$)		RMS($\ddot{\mathbf{z}}$)	
z_1 (m)	0.0149 •	$\dot{z}_1$ (m/s)	0.0784 ↓	$\ddot{z}_1$ (m/s^2)	0.6180 ↓
z_2 (m)	0.0126 •	$\dot{z}_2$ (m/s)	0.0455 ↓	$\ddot{z}_2$ (m/s^2)	0.6709 ↓
z_3 (rad)	0.0022 •	$\dot{z}_3$ (rad/s)	0.0217 ↓	$\ddot{z}_3$ (rad/s^2)	0.5386 ↓
z_4 (rad)	0.0155 •	$\dot{z}_4$ (rad/s)	0.0568 ↓	$\ddot{z}_4$ (rad/s^2)	0.7975 ↓
z_5 (m)	0.0158 •	$\dot{z}_5$ (m/s)	0.2310 ↑	$\ddot{z}_5$ (m/s^2)	22.5142 ↑
z_6 (m)	0.0152 •	$\dot{z}_6$ (m/s)	0.1144 ↑	$\ddot{z}_6$ (m/s^2)	5.5945 ↑
z_7 (m)	0.0152 •	$\dot{z}_7$ (m/s)	0.1258 ↑	$\ddot{z}_7$ (m/s^2)	6.0624 ↑
z_8 (m)	0.0160 •	$\dot{z}_8$ (m/s)	0.2599 ↑	$\ddot{z}_8$ (m/s^2)	19.3652 ↑

to the time histories of the dynamic amplification factors of each wheel of the model, which translates into a preservation of these factors below unity and maintenance of the risk of loss of contact between the tire and the road. Additionally, it can be observed that the third objective function increased from 32.87 to 35.17 mm, i.e., by 7%. Even with this increase, the value of the third objective function is still well below 127 mm, considered by Gillespie (2010) to be the smallest suspension stroke normally found in compact cars.

Naudé and Snyman (2003a, b) state that full 3D models are typically used by research and development centers of original equipment manufacturers, and that simpler 2D models are mandatory for economically useful coupling with their

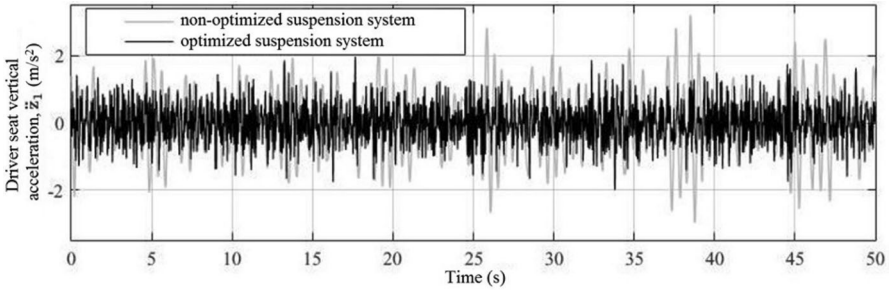

Fig. 5 Time histories of the driver seat vertical acceleration

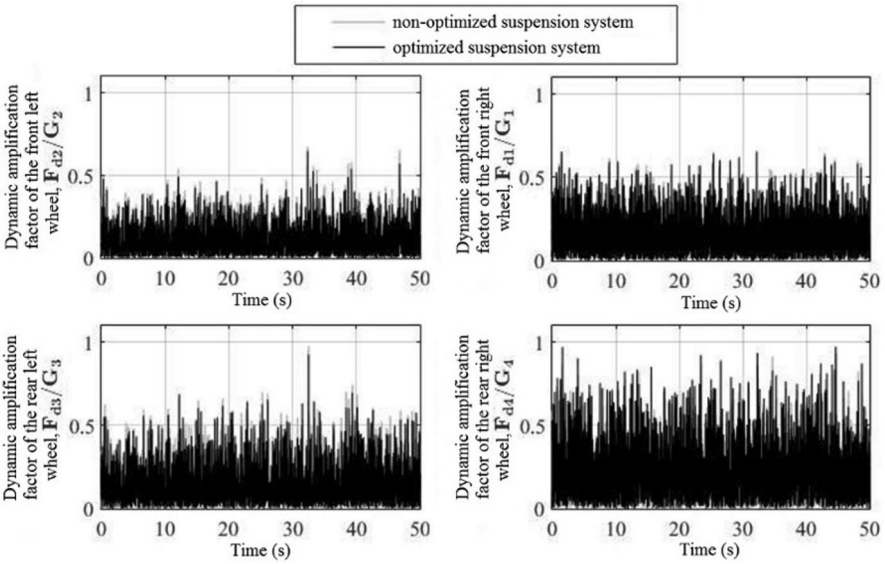

Fig. 6 Time histories of the dynamic amplification factors of the front right, front left, rear left and rear right wheel of the vehicle model

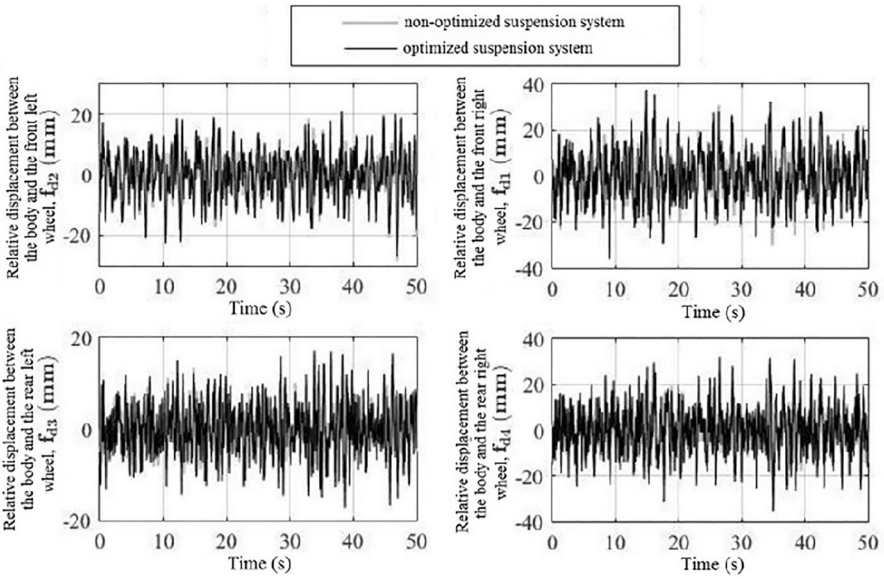

Fig. 7 Time histories of the relative displacements between the body and front right, front left, rear left and rear right wheel of the vehicle model

Table 17 Mean values of the components of the objective vector of the optimization problem

	$\mu[F_T(\mathbf{x_R})]$		$\mu[F_T(\mathbf{x_{TP}})]$	Difference between $\mu[F_T(\mathbf{x_R})]$ and $\mu[F_T(\mathbf{x_{TP}})]$ (%)
$F_{T1}(\mathbf{x_R})$ (m/s^2)	0.2625	$F_{T1}(\mathbf{x_{TP}})$ (m/s^2)	0.2070	− 21.14
$F_{T2}(\mathbf{x_R})$	0.1811	$F_{T2}(\mathbf{x_{TP}})$	0.1806	− 0.28
$F_{T3}(\mathbf{x_R})$ (mm)	32.87	$F_{T3}(\mathbf{x_{TP}})$ (mm)	35.17	7.00

gradient-based optimization tool. The present work, however, was successful in coupling a full 3D vehicle model with the NSGA-II multi-optimization algorithm without making the problem computationally intractable. This demonstrates the advantages of using metaheuristic algorithms for the solution of such problems.

5 Conclusions

We have proposed an effective methodology for the optimal design of the passive suspension system of a full-car model randomly excited. We developed a numerical-computational routine for dynamic and modal analyses of the full-car model, integrated with NSGA-II, to perform the multi-objective optimization of the suspension parameters.

The numerical results demonstrated that the multi-objective optimization method is capable of generating a Pareto-optimal front using the dynamic analysis methodology proposed in the present study. This 3D front has proven to be an excellent support tool to aid the designer in the determination of the parameters that best fit the suspension system to produce the desired dynamic behavior.

By comparing the results of the dynamic analyses of the vehicle model with optimized and non-optimized suspension systems, we showed that the optimization allowed a reduction of up to 21.14% of the weighted RMS value of the driver seat vertical acceleration, a parameter directly related to comfort, while maintaining or improving the trade-off with safety. This improvement highlights the effectiveness of our multi-objective optimization routine.

Thus, the proposed optimization methodology can be recommended as an effective tool for the optimal design of passive suspension system parameters. Finally, this paper shows that the design of the suspension parameters can simultaneously take into account passenger comfort and safety.

Acknowledgements The authors acknowledge the financial support of the funding agencies CNPq and CAPES from Brazil.

References

Abbas W, Emam A, Badran S, Shebl M, Abouelatta O (2013) Optimal seat and suspension design for a half-car with driver model using genetic algorithm. Lect Notes Control Inf 4(2):199–205

Bianchi L, Dorigo M, Gambardella LM, Gutjahr WJ (2009) A survey on metaheuristics for stochastic combinatorial optimization. Nat Comput 8:239–287

Braun H (1991) Meßergebnisse von straßenunebenheiten, VDI-Berichte 877, Düsseldorf, Germany

Deb K, Pratap A, Agarwal S, Meyarivan T (2002) A fast and elitist multiobjective genetic algorithm: NSGA-II. IEEE Trans Evolut Comput 6(2):182–197

Dodds CJ, Robson JD (1973) The description of road surface roughness. J Sound Vib 31(2):175–183

Drehmer LRC, Casas WJP, Gomes HM (2015) Parameters optimisation of a vehicle suspension system using a particle swarm optimisation algorithm. Veh Syst Dyn 53:449–474

Eberhart R, Kennedy J (1995) A new optimizer using particle swarm theory. In: Proceedings of the international symposium on micro machine and human science, Nagoya, Japan, 4–6 Oct

Fadel Miguel LF, Lopez RH, Miguel LFF (2013) Multimodal size, shape, and topology optimisation of truss structures using the Firefly algorithm. Adv Eng Softw 56:23–37. https://doi.org/10.1016/j.advengsoft.2012.11.006

Florea A, Cofaru II, Roman L, Cofaru N (2016) Applying the multi-objective optimization techniques in the design of suspension systems. J Digit Inf Manag 14(6):351–367

Gadhvi B, Savsani V, Patel V (2016) Multi-objective optimization of vehicle passive suspension system using NSGA-II, SPEA2 and PESA-II. Procedia Technol 23:361–368

Gandomi AH, Talatahari S, Tadbiri F, Alavi AH (2013) Krill herd algorithm for optimum design of truss structures. Int J Bio-Inspired Comput 5(5):281–288. https://doi.org/10.1504/ijbic.2013.057191

Geem ZW, Kim JH, Loganathan GV (2001) A new heuristic optimization: harmony search. Simulation 76:60–68

Gillespie TD (2010) Fundamentals of vehicle dynamics. Society of Automotive Engineers, Warrendale

Gobbi M (2013) A k, k − ε optimality selection based multi objective genetic algorithm with applications to vehicle engineering. Optim Eng 14:345–360

Gobbi M, Mastinu G (2001) Analytical description and optimization of the dynamic behaviour of passively suspended road vehicles. J Sound Vib 245(3):457–481

Gobbi M, Levi F, Mastinu G (2006) Multi-objective stochastic optimisation of the suspension system of road vehicles. J Sound Vib 298(4–5):1055–1072

Gobbi M, Guarneri P, Scala L, Scotti L (2014) A local approximation based multi-objective optimization algorithm with applications. Optim Eng 15:619–641

Griffin MJ (1990) Handbook of human vibration. Elsevier Academic Press, London

Guclu R (2005) Fuzzy logic control of seat vibrations of a non-linear full vehicle model. Nonlinear Dyn 40:21–34

Guo P, Zhang JH (2017) Numerical model and multi-objective optimization analysis of vehicle vibration. J Zhejiang Univ-Sci A 18(5):393–412

Holland JH (1975) Adaptation in natural and artificial systems. The University of Michigan Press, Ann Arbor

International Organization for Standardization, ISO 2631-1 (1997) Mechanical vibration and shock—evaluation of human exposure to whole-body vibration, Switzerland

International Organization for Standardization, ISO 8608 (2016) Mechanical vibration—road surface profiles reporting of measured data, Switzerland

Jamali A, Shams H, Fasihozaman M (2014) Pareto multi-objective optimum design of vehicle-suspension system under random road excitations. Proc Inst Mech Eng Part K J Multi-body Dyn 228(3):282–293

Khalkhali A, Sarmadi M, Yousefi S (2017) Reliability-based robust multi-objective optimization of a 5-DOF vehicle vibration model subjected to random road profiles. J Cent South Univ 24(1):104–113

Meng R, Xie NG, Wang L (2014) Multiobjective game method based on self-adaptative space division of design variables and its application to vehicle suspension. Math Probl Eng. https://doi.org/10.1155/2014/479272

Miguel LFF, Fadel Miguel LF (2012) Shape and size optimization of truss structures considering dynamic constraints through modern metaheuristic algorithms. Expert Syst Appl 39:9458–9467. https://doi.org/10.1016/j.eswa.2012.02.113

Moradi A, Nafchi AM, Ghanbarzadeh A, Soodmand E (2011) Optimization of linear and nonlinear full vehicle model for improving ride comfort vs. road holding with the Bees Algorithm. In: Proceedings of the IEEE colloquium on humanities, science and engineering research, Penang, Malaysia, 5–6 Dec

Nagarkar MP, Patil GJV, Patil RNZ (2016) Optimization of nonlinear quarter car suspension seat-driver model. J Adv Res 7(6):991–1007

Nariman-Zadeh N, Salehpour M, Jamali A, Haghgoo E (2010) Pareto optimization of a five-degree of freedom vehicle vibration model using a multi-objective uniform-diversity genetic algorithm (MUGA). Eng Appl Artif Intel 23(4):543–551

Naudé AF, Snyman JA (2003a) Optimization of road vehicle passive suspension systems. Part 1. optimization algorithm and vehicle model. Appl Math Model 27:249–261

Naudé AF, Snyman JA (2003b) Optimization of road vehicle passive suspension systems. Part 2. qualification and case study. Appl Math Model 27:263–274

Ngwangwa HM, Heyns PS, Breytenbach HGA, Els PS (2014) Reconstruction of road defects and road roughness classification. J Terramech 53:1–18

Sekulic D, Dedovic V, Rusov S, Salinic S, Obradovic A (2013) Analysis of vibration effects on the comfort of intercity bus users by oscillatory model with ten degrees of freedom. Appl Math Model 37:8629–8644

Shinozuka M, Jan CM (1972) Digital simulation of random process and its applications. J Sound Vib 25:111–118

Shirahatt A (2015) Analysis and simulation of active suspension system for full vehicle model subjected to random road profile. Int J Innov Res Sci Eng Technol 4(1):18489–18502

Shirahatt A, Prasad PSS, Panzade P, Kulkarni MM (2008) Optimal design of passenger car suspension for ride and road holding. J Braz Soc Mech Sci 30(1):66–76

Shojaeefard MH, Khalkhali A, Erfani PS (2014) Multiobjective suspension optimization of a 5-DOF vehicle vibration model excited by random road profile. Int J Adv Des Manuf Technol 7(1):1–7

Song C, Zhao Y, Wang L, Niu L (2014) Multi-objective optimization design of passive suspension parameters based on competition-cooperation game model. Aust J Mech Eng 12(1):13–24

Wang L, Xie NG, Song CZ, Bao JH, Cen YW (2010) Multi-objective bionics design method of passive suspension parameters based on hybrid behavior game. Struct Multidiscip Opt 42(3):371–386

Xie NG, Meng R, Ye Y, Wang L, Cen YW (2013) Multiobjective design method based on evolution game and its application for suspension. Struct Multidiscip Opt 47(2):207–220

Yang XS (2010) Firefly algorithm, stochastic test functions and design optimization. Int J Bio-Inspired Comput 2(2):78–84

Yang XS, Deb S (2010) Engineering optimization by cuckoo search. Int J Math Model Numer Optim 1:330–343

Affiliations

Giovani Gaiardo Fossati[1] · Letícia Fleck Fadel Miguel[1] · Walter Jesus Paucar Casas[1]

Giovani Gaiardo Fossati
gfossati26@gmail.com

Walter Jesus Paucar Casas
walter.paucar.casas@ufrgs.br

[1] Department of Mechanical Engineering, Federal University of Rio Grande do Sul, Rua Sarmento Leite 425, Porto Alegre, RS 90050-170, Brazil